Effects of preparation parameters on growth and properties of β-Ga_2O_3 film

Zi-Hao Chen(陈子豪), Yong-Sheng Wang(王永胜)†, Ning Zhang(张宁), Bin Zhou(周兵), Jie Gao(高洁), Yan-Xia Wu(吴艳霞), Yong Ma(马永), Hong-Jun Hei(黑鸿君), Yan-Yan Shen(申艳艳), Zhi-Yong He(贺志勇), and Sheng-Wang Yu(于盛旺)

College of Materials Science and Engineering, Taiyuan University of Technology, Taiyuan 030024, *China*

(Received 13 February 2022; revised manuscript received 23 May 2022; accepted manuscript online 24 May 2022)

The Ga_2O_3 films are deposited on the Si and quartz substrates by magnetron sputtering, and annealing. The effects of preparation parameters (such as argon–oxygen flow ratio, sputtering power, sputtering time and annealing temperature) on the growth and properties (*e.g.*, surface morphology, crystal structure, optical and electrical properties of the films) are studied by x-ray diffractometer (XRD), scanning electron microscope (SEM), and ultraviolet-visible spectrophotometer (UV-Vis). The results show that the thickness, crystallization quality and surface roughness of the β-Ga_2O_3 film are influenced by those parameters. All β-Ga_2O_3films show good optical properties. Moreover, the value of bandgap increases with the enlarge of the percentage of oxygen increasing, and decreases with the increase of sputtering power and annealing temperature, indicating that the bandgap is related to the quality of the film and affected by the number of oxygen vacancy defects. The *I*–*V* curves show that the Ohmic behavior between metal and β-Ga_2O_3 films is obtained at 900 °C. Those results will be helpful for the further research of β-Ga_2O_3 photoelectric semiconductor.

Keywords: β-Ga_2O_3, magnetron sputtering, growth parameters, optical and electrical properties

PACS: 73.20.At, 81.15.Cd, 85.60.Gz **DOI:** 10.1088/1674-1056/ac728c

1. Introduction

With the excellent physicochemical properties, the wide bandgap semiconductor materials (such as SiC, GaN, AlGaN) are very suitable for high-temperature, high-frequency, and high-power semiconductor devices including diodes, detectors, and high-power electronic devices.[1–3] However, these devices are rarely able to go out of the laboratory and enter into industrialization because of the high cost of fabrication. Therefore, to reduce the cost of wide bandgap semiconductor devices is necessary for their practical application. As a wide bandgap semiconductor, Ga_2O_3 has a band gap of $\sim$ 4.9 eV, a Baliga's figure of merit (BFOM) of 3400, and a breakdown field strength of 8 MV/cm.[4] Compared with SiC or GaN, the single-crystal Ga_2O_3 wafer with a size of 4 inch (1 inch = 2.54 cm) has been synthesized by using several standard melt growth methods.[5] The polycrystalline Ga_2O_3 film has similar semiconductor characteristics to and lower fabrication cost than single crystal, these advantages make Ga_2O_3 receive increasing attention in the field of electroluminescent devices,[6,7] gas sensitive sensors,[8–10] photodetectors,[11–13] field-effect transistor,[14–16] *etc*.

The crystal structures of Ga_2O_3, including α, β, γ, δ, and ε, could transform into each other under given conditions.[17] Among them, defects in the growth of β-Ga_2O_3 thin film include V_O (oxygen vacancy), O_i (oxygen interstitial), V_{Ga} (gallium vacancy), and Ga_i (gallium interstitial) due to a monoclinic crystal with the $C2/m$ space group. Owing to the V_O and Ga_i with the lower formation energy,[18] β-Ga_2O_3 is prone to forming oxygen vacancies and gallium interstitial during growth. Therefore, the β-Ga_2O_3, as a most stable phase, has aroused extensive interest in the semiconductor devices due to its promising future in the industrial application. Sasaki *et al*. found that the Pt/β-Ga_2O_3 Schottky diode fabricated by the floating-zone has a Schottky barrier height in a range of 1.3 eV–1.5 eV.[19] Shimbori *et al*. reported that NiO/β-Ga_2O_3 heterojunction diode has a higher breakdown voltage and lower leakage current than Ni/β-Ga_2O_3 Schottky diodes.[20] Oh *et al.* reported that a β-Ga_2O_3 MSM photodetector with the transparent graphene electrode increases the photosensitive area and rejection ratio of the photodetector.[21] Zhang *et al*. reported that single-crystalline spherical β-Ga_2O_3 particles with an average diameter of $\sim$ 200 nm are expected to be used in white-LED phosphors due to the blue–green and red–light emission.[22] Many methods have been used to prepare the β-Ga_2O_3 film and adjust defects. Green *et al*. found that the β-Ga_2O_3 field-effect transistor fabricated by metal–organic vapor phase epitaxy has a gate-to-drain electric field of $\sim$ 3.8 MV/cm.[23] Moreover, Chen *et al*. found that the growth of β-Ga_2O_3 film is dependent on the oxygen pressure of pulsed laser deposition, such as mainly along (201) plane at an oxygen pressure of 0.5 Pa, but along (400) plane for oxygen pressure in a range from 0.5 Pa to 2 Pa.[24] Chen *et al*. reported that the pressure of β-Ga_2O_3 film can affect the preferred orientation and growth rate by metal–organic chemical vapor deposition on GaAs substrate.[25] Shih *et al*. found that the β-Ga_2O_3 MOS-HEMT has excellent performance caused by β-Ga_2O_3 gate dielectric and surface passivation layer.[26]

†Corresponding author. E-mail: wangyongsheng@tyut.edu.cn

© 2023 Chinese Physical Society and IOP Publishing Ltd

Liao *et al*. found that the crystal quality of β-Ga_2O_3 film can be adjusted by RF magnetron sputtering under growth pressure in a range of 0.5 Pa–3 Pa, resulting in a similar variation trend to that of the optical bandgap of β-Ga_2O_3 film.[27] Ma and Fan prepared β-Ga_2O_3 nanomaterials by the thermal evaporation method, and found that the photoelectric properties of the nanomaterials change due to the oxygen existing.[28] Based on these results, the preparation method and parameter have important effects on the growth and properties of the β-Ga_2O_3 film.

In this work, the Ga_2O_3 films are prepared on the silicon and quartz substrates by radio frequency (RF) magnetron sputtering, then transformed into β-Ga_2O_3 by annealing. The effects of preparation parameters on the structure and properties of β-Ga_2O_3 film are studied by tailoring argon–oxygen flow ratio, sputtering power, sputtering time and annealing temperature.

2. Experimental details

The Ga_2O_3 films were fabricated on the surface of (100) silicon substrates by the RF magnetron sputtering method. The monocrystalline silicon wafers were ultrasonically cleaned in ethanol solution for 10 min and washed with deionized water and dried, then placed into the deposition chamber of magnetron sputtering apparatus. In order to remove impurities from the surface of gallium oxide target as much as possible, the pre-sputtering was carried out in argon atmosphere for 5 min, then the presetting sputtering power and gas flow were adjusted. The atmospheric pressure of the chamber was adjusted to 0.8 Pa by controlling the outlet valve. A small amount of O_2 is added in addition to argon to improve crystallinity of the film and reduce internal defects.[29] Under the combined action of electric field, magnetic field and argon particles, gallium particles in the target were bombarded and reacted with oxygen to form amorphous Ga_2O_3 film on the substrate. The β-Ga_2O_3 film was obtained after being annealed.[30] The effects of preparation parameters including argon–oxygen flow ratio, sputtering power, sputtering time and annealing temperature on the growth and properties of β-Ga_2O_3 thin films were studied as shown in Table 1. All samples were annealed in air for 120 min. In each experiment, a quartz substrate (optical transmittance $> 90\%$) was placed in the sputtering system so as to be used for characterizing the optical properties of the films.

Table 1. Detailed growth parameters of β-Ga_2O_3 thin films. AO: argon–oxygen flow ratio, SP: sputtering power, Pre: sputtering pressure, ST: sputtering time, AT: annealing temperature.

Group	Variables	Parameters	Constants
1	AO	4:1	SP: 200 W
		5:1	Pre: 0.8 Pa
		8:1	ST: 120 min
		10:1	AT: 600 °C
2	SP (W)	140	AO: 8:1
		160	Pre: 0.8 Pa
		180	ST: 120 min
		200	AT: 600 °C
3	ST (min)	60	AO: 8:1
		90	Pre: 0.8 Pa
		120	SP: 200 W
		150	AT: 600 °C
4	AT (°C)	600	AO: 8:1
		700	Pre: 0.8 Pa
		800	SP: 200 W
		900	ST: 120 min

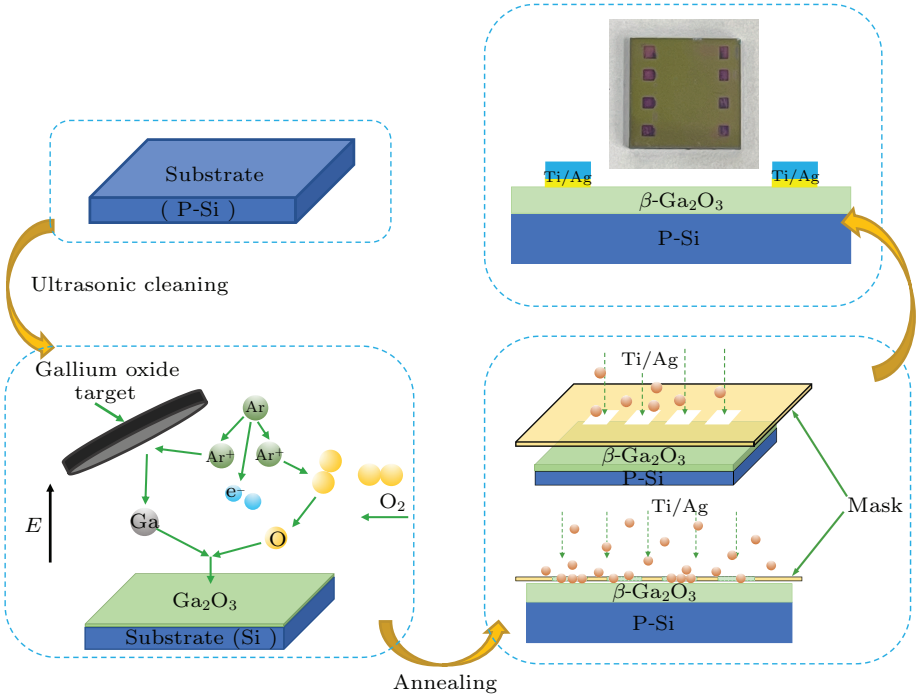


Fig. 1. Schematic diagram of preparation process of β-Ga_2O_3 thin films.

The metal electrodes were prepared on the film to study the electrical property. The β-Ga_2O_3 film samples were ultrasonically cleaned in ethanol solution for 5 min, then rinsed with deionized water and dried. The Ti could form Ohmic contact with β-Ga_2O_3 under a certain condition.[31] The metal electrodes were obtained by depositing Ti (40 nm)/Ag (80 nm) on the surface of sample by vacuum evaporation via a special mask. Each electrode has a size of 1 mm×1 mm and the spacing between adjacent electrodes is 2 mm. The samples with metal electrodes were annealed in air for 30 s at 400 °C. Figure 1 shows a schematic diagram of the preparation process and the final product.

The crystal structure of β-Ga_2O_3 were characterized by x-ray diffraction (XRD, Smartlab X, Rigaku). The morphology of β-Ga_2O_3 and Ti/Ag electrodes were characterized by scanning electron microscope (SEM, ZEISS GeminiSEM 300). The optical properties were obtained by UV-vis spectrophotometer (Agilent cary 100). The *I*–*V* curve of the films were measured by Hall effect measurement (Lake shore 8400 Series).

3. Results and discussion

Figure 2 shows the XRD patterns of Ga_2O_3 films deposited under different conditions. The broad diffraction patterns of Ga_2O_3 samples indicate the amorphous structures under different argon–oxygen flow ratios (Fig. 2(a)). The obvious diffraction peaks at 30.5°, 35.2°, and 64.7° correspond to ($\bar{4}01$), (111), and (403) planes of β-Ga_2O_3 by examining the standard card of JCPDS43-1012, and superimpose on the broad diffraction pattern of the amorphous Ga_2O_3, suggesting that the amorphous Ga_2O_3 films have transformed into β phase after being annealed. The oxygen content increases with the argon–oxygen flow ratio dropping, leading to the shift of diffraction peak in the crystal plane of (403). The crystal lattice contains the increased amount of V_O under the hypoxia environment, and in an oxygen-rich environment, enough oxygen atoms exist as O_i, leading to the lattice distortion. When the sputtering power is 140 W (Fig. 2(b)), the crystal plane of ($\bar{4}01$) dominates the process of crystallization. With the increase of sputtering power, the diffraction peak in the crystal plane of (111) instead of in the crystal plane of ($\bar{4}01$) is enhanced, indicating the preferential growth of the film. According to the Scherrer formula[32]

$$D = k\lambda / B\cos\theta, \tag{1}$$

where D is the grain size perpendicular to the lattice plane, k is the Scherrer constant with a value of 0.9, λ is the wavelength of x-ray radiation, B is the full width at half maximum (FWHM) of diffraction peaks, and θ is the corresponding Bragg angle. Here, the FWHM of the diffraction peak at crystal plane of ($\bar{4}01$) increases with the augment of sputtering power (Fig. 2(b)), indicating that the grain size decreases. The increase of sputtering power leads to a strong bombardment effect. So, more atoms bombarded out of Ga_2O_3 target result in more deposited-nanocrystals.

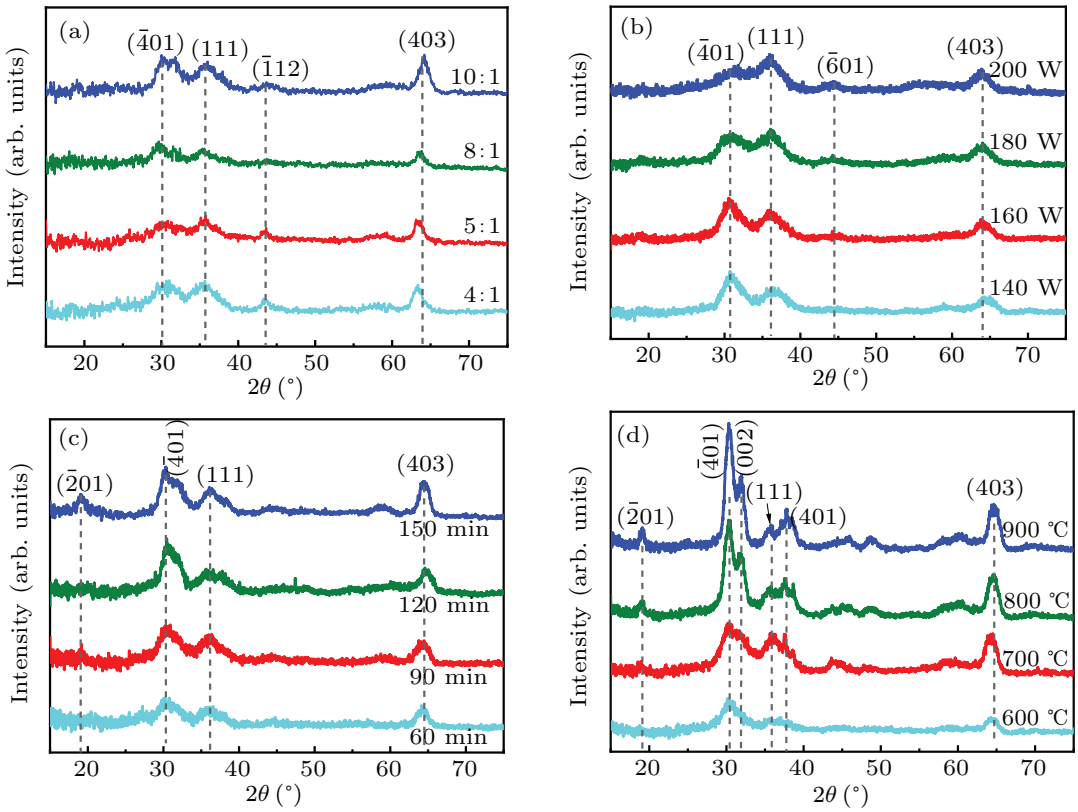


Fig. 2. XRD patterns of β-Ga_2O_3 films deposited under different parameters: (a) argon–oxygen flow ratio; (b) sputtering power; (c) sputtering time; (d) annealing temperature.

Moreover, as the sputtering time increases (Fig. 2(c)), the intensities of diffraction peaks increase. Specially, the diffraction peaks appear at 19.0° and 59.2° corresponding to the crystal planes of $(\bar{2}01)$ and $(\bar{6}03)$ for 150 min. As for samples of the different annealing temperatures (Fig. 2(d)), the diffraction peaks at 30.5° and 64.7° superimpose on the broad diffraction pattern of the amorphous Ga_2O_3 for sample annealed at 600 °C. With the temperature increasing to 900 °C, the diffraction peaks are enhanced in (111), $(\bar{2}01)$, (002), and (401) crystal planes. We find that each crystal plane of all samples annealed at 600 °C shows the low diffraction peak intensity and the large FWHM, but the diffraction peak intensity of samples annealed at 900 °C all increase (Figs. 2(a)–2(d)). It means that the crystallinity of β-Ga_2O_3 films increases with the annealed temperature rising.

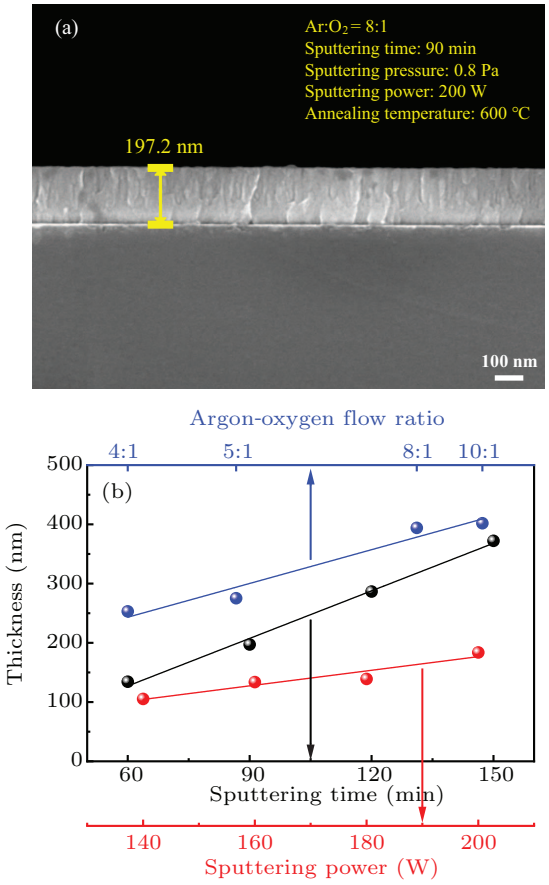


Fig. 3. (a) Cross-sectional SEM image of β-Ga_2O_3 film and (b) plot of thickness *versus* sputtering time, sputtering power, and argon–oxygen flow rate of β-Ga_2O_3 film.

Figure 3(a) shows the cross-sectional morphology of β-Ga_2O_3 film. The β-Ga_2O_3 film has the uniform and dense cross-sectional morphology without internal holes. Under this preparation condition, the thickness of the β-Ga_2O_3film is 197.2 nm. Moreover, the thickness values of the β-Ga_2O_3 films at various preparation parameters are summarized via the cross-sectional image (Fig. 3(b)). Obviously, the thickness of the β-Ga_2O_3 film increases with the increase of the argon–oxygen flow ratio, sputtering power and time. The annealing temperature has almost no influence on the thickness of the film (not shown). With the enlargement of argon–oxygen flow ratio, more argon particles bombard Ga_2O_3 target, resulting in the increase of growth rate. Moreover, with the increase of sputtering power, more Ga_2O_3 particles are generated and react with the oxygen due to the enhanced bombardment effect on the Ga_2O_3 target, resulting in the increased thickness of the film.

Figure 4(a) shows the surface morphologies of β-Ga_2O_3 films annealed at different temperatures. The flat surface morphologies of films annealed at 600 °C shows small grains of Ga_2O_3, which are due to the incomplete crystallization. The formation of small nanocrystalline grains for β-Ga_2O_3 can be confirmed by the weaker diffraction peak intensity and larger FWHM (Fig. 2(d)). With the increase of annealing temperature, the crystallinity of the film can be greatly improved, and the obvious spherical protrusions can be observed on the surface of sample annealed at 800 °C. When the annealing temperature is further increased to 900 °C, the spherical grains on the surface become dense, and more spherical grains with diameters ranging from 20 nm to 30 nm form.

The 3D contour image of the sample surface is characterized, and the roughness-related parameters are obtained as follows: average roughness (R_a), maximum peak of contour (R_p) and minimum valley of contour (R_v). Figure 4(b) shows the 3D contour image of the sample annealed at 600 °C, the overall surface of the film is smooth and flat without obvious pits and spikes, which is consistent with the scenario of SEM image in Fig. 4(a). With the enlargement of argon–oxygen flow ratio (Fig. 4(c)), the R_a of the film first decreases, then increases. A minimum R_a-value can be obtained at an argon–oxygen flow ratio of 8:1. The higher R_a-value means the oxygen-deficient situation, which is caused by stronger bombardment of the film surface at low oxygen content. The growth rate of β-Ga_2O_3 thin film slows down with the increase of oxygen content. Moreover, the oxygen-rich environment reduces surface defects of the films. However, with the increase of sputtering power, the R_a-value decreases by nearly half, thus improving the surface quality. The increased sputtering power means the strengthening of bombardment effect, which improves the adatom mobility and contributes to the surface quality of film. There has little effect on the R_a-values of samples annealed at different temperature, but the values of R_p and R_v increase with the annealing temperature increasing (R_p : 7.8 nm→ 145.9 nm; R_v: 43.5 nm→ −245.2 nm). With the increase of sputtering time, the R_a of β-Ga_2O_3 thin film increases gradually to 2.8 nm at 150 min. The increase of time can lead to the accumulation of defects to accumulate, resulting in uneven distribution of grains on the surface.

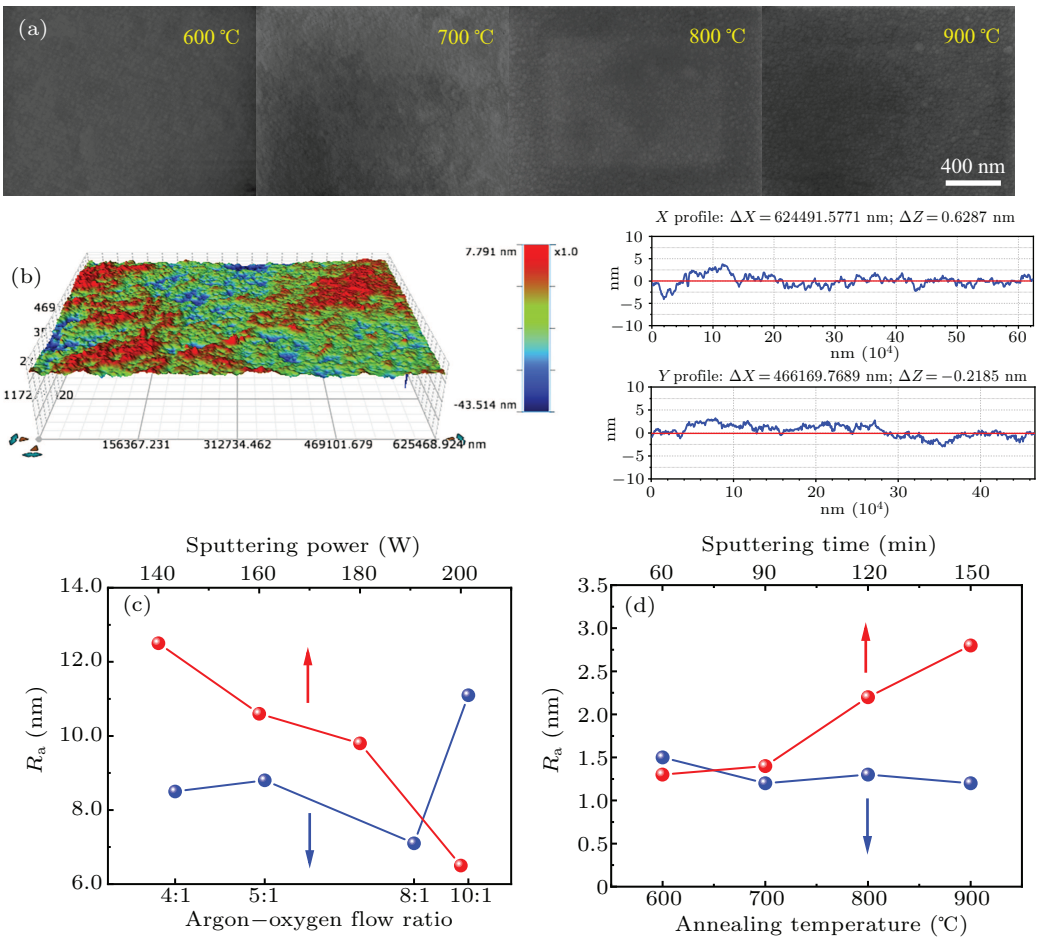


Fig. 4. (a) Top-view SEM images of β-Ga_2O_3 thin films annealed at different temperatures, (b) three-dimensional (3D) contour image of β-Ga_2O_3 thin film annealed at 600 °C for 120 min, (c) plot of average roughness (R_a) *versus* argon–oxygen flow ratio and sputtering power, and (d) plot of average roughness *versus* annealing temperature and sputtering time of β-Ga_2O_3 thin films.

Figure 5(a) shows the SEM cross-section image of the prepared electrode structure. By combining the EDS results of the cross-section (Fig. 5(b)), the obvious layered structure of Ag/Ti/Ga_2O_3/Si-substrate can be confirmed. The O element not only exists in the gallium layer, but also penetrates into the Si layer and diffuses into the Ti/Ag electrode after being annealed (EDS result). In addition, Si also diffuses toward the Ga_2O_3 layer, which has a similar mechanism to that of Si doped β-Ga_2O_3 affecting the bandgap of β-Ga_2O_3 thin films.

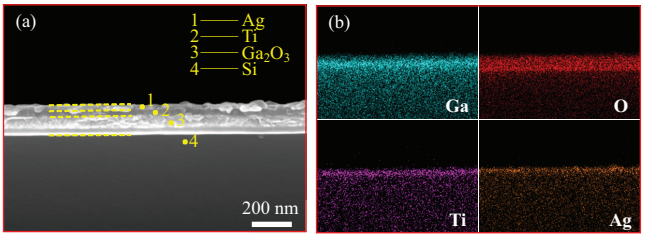


Fig. 5. (a) Cross-section SEM image of prepared electrode structure, and (b) corresponding EDS mapping element distributions.

Figure 6 shows the optical transmittance spectra of current β-Ga_2O_3 films at different preparation parameters. All β-Ga_2O_3 films display the good optical transmittances in the visible range of 380 nm–780 nm. An obvious absorption edge appears near to 250 nm, which indicates that β-Ga_2O_3 films are suitable for the detection of UVC. Fabry–Perot oscillation of the transmission curve implies good interface quality between β-Ga_2O_3 films and substrates.[33] The optical transmittance of the film is enhanced with the increase of sputtering power and annealing temperature, which is related to the improvement of film quality. Moreover, it is notable that the absorption edge has a red shift with the increase of sputtering time and power. Since main defects of V_O accumulate in the process of deposition and growth of film, these V_O exist in the energy band as the donor energy, leading to the shifting of band structure. As Li *et al.*[34] believed, that was a degradation of quantum size effect. Because β-Ga_2O_3 is a direct bandgap semiconductor,[35] the bandgap of β-Ga_2O_3thin film can be calculated from Tauc formula[36]

$$(\alpha h\nu)^2 = A(h\nu - E_g), \tag{2}$$

where α is the absorption coefficient, $h\nu$ is the incident photon energy, A is the constant, and E_g is the bandgap, the value of E_g can be derived by fitting the linear region of the $(\alpha h\nu)^2$ *versus* $h\nu$ plot and taking the intercept on the $h\nu$-axis (Fig. 6). Here, the bandgap of the β-Ga_2O_3 decreases with the decrease of oxygen, which can be attributed to the increase of point defects dominated by oxygen vacancies. In addition, the bandgap also gradually decreases with the increase of sputtering power and

annealing temperature. In short, the surface quality can be improved by increasing the sputtering power, resulting in the reducing bandgap; the crystal quality increases with the increase of temperature, leading to the decrease of bandgap. All these results indicate that the bandgap of β-Ga_2O_3 films is affected by the film quality.

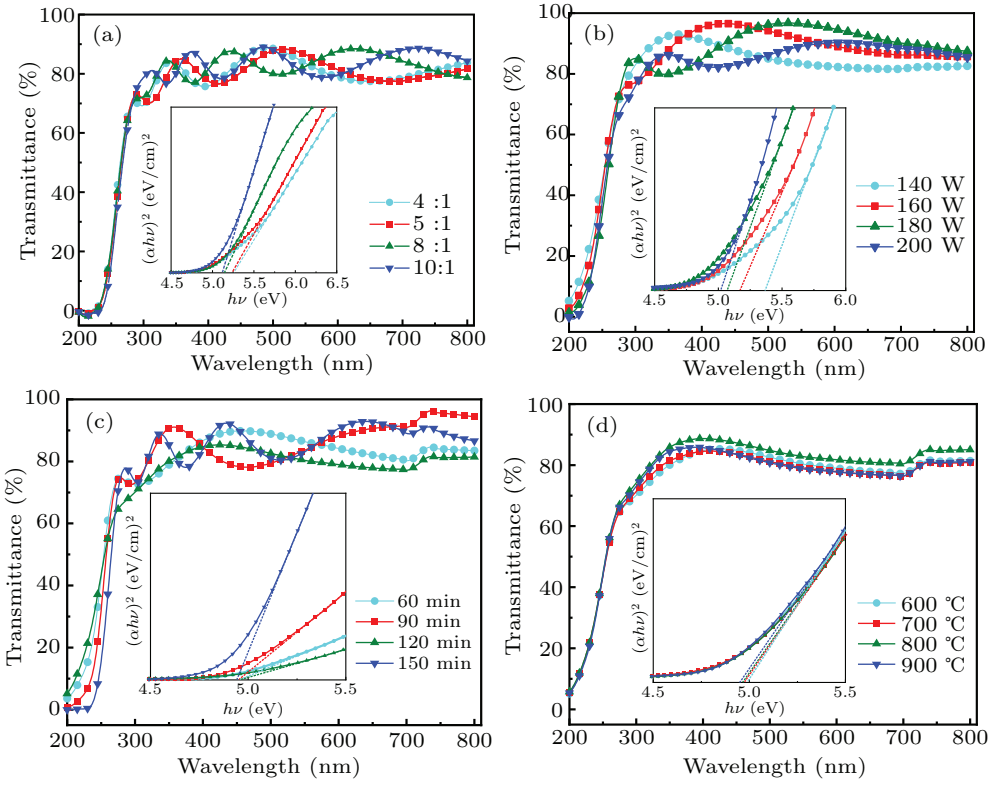


Fig. 6. Variations of optical transmittance spectra of β-Ga_2O_3thin films: with (a) argon–oxygen flow ratio, (b) sputtering power, (c) sputtering time, and (d) annealing temperature, with inset showing variations of $(\alpha h\nu)^2$ with photon energy $(h\nu)$.

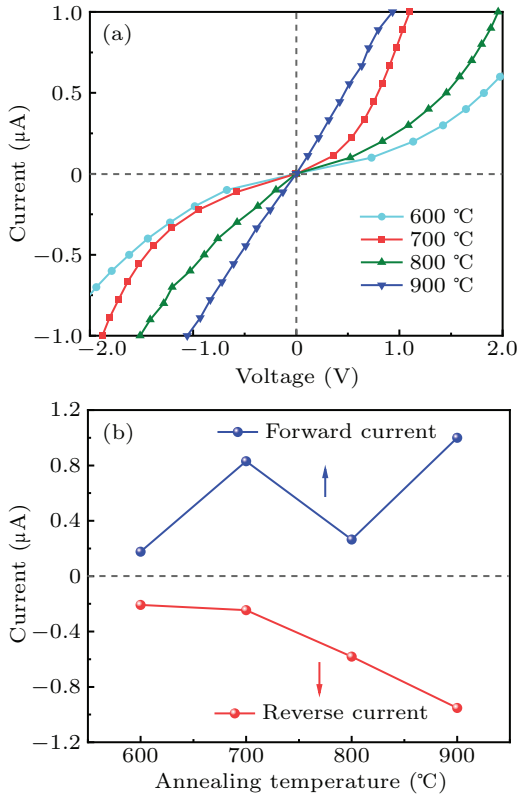


Fig. 7. (a) The *I*–*V* curves of β-Ga_2O_3 thin films annealed at different temperatures and (b) current flowing through the thin film *versus* annealing temperature at a bias voltage of 1 V.

The *I*–*V* curves of β-Ga_2O_3 thin films at different growth parameters are tested. The sample annealed at 900 °C shows the Ohmic behavior between Ti and β-Ga_2O_3, and the remaining samples exhibit the Schottky contact behavior (Fig. 7(a)). Moreover, the forward/reverse current at 1-V bias voltage are calculated (Fig. 7(b)). The current flowing through the β-Ga_2O_3 film increases almost with the increase of annealing temperature, indicating that the resistance of the film gradually decreases. It is closely related to the crystallization quality of the film (Fig. 2(d)). There is a higher intensity of diffraction peak and a smaller FWHM at 900 °C, thus the currents can flow across the grain boundaries.[37]

The E_g-values obtained at different preparation parameters are calculated in Fig. 8(a). The E_g-value represents the distance from the top of valence band to the bottom of conduction band in the band structure, which varies from 4.94 eV to 5.34 eV depending on the preparation process. However, almost all samples (except for the sample annealed at 900 °C) are of Schottky contact, indicating that the formation of Ohmic contact is not just related to the band gap of the film. In fact, for n-type intrinsic semiconductor such as β-Ga_2O_3, the formation of Ohmic contact depends on the Schottky barrier height ϕ_B:

$$\phi_B = \phi_M - \chi_s, \tag{3}$$

where ϕ_M is the metal work function, and χ_s is the electron

affinity of the semiconductor. Usually, the ϕ_B with a negative value is achieved by choosing a metal of low ϕ_M at the constant χ_s (4.00±0.05 eV), named Ohmic contact.[38] However, the ϕ_B of β-Ga_2O_3 does not rely on ϕ_M directly because of the surface states, metal-induced gap-states and near surface defects.[39] Previous report found that there can be the upward bending of the band on β-Ga_2O_3 surface,[40] causing the contacts formed between β-Ga_2O_3 and metals to be always Schottky contacts (Fig. 8(b)). The Ohmic contact between the metal and β-Ga_2O_3 forms at 900 °C temperature. As mentioned above, the point defects in β-Ga_2O_3 film are dominated by oxygen vacancies, thus introducing additional defect levels into the band structure. However, it is too deep to be excited according to previous report, so it is not generally considered to be the source of charge carriers. When the annealing temperature reaches 900 °C, the high temperature provides a large amount of energy for the thermal motion of the electrons, thus leading a large number of electrons to be excited and transit to the conduction band. So, the Ohmic contact is achieved through the tunneling effect.

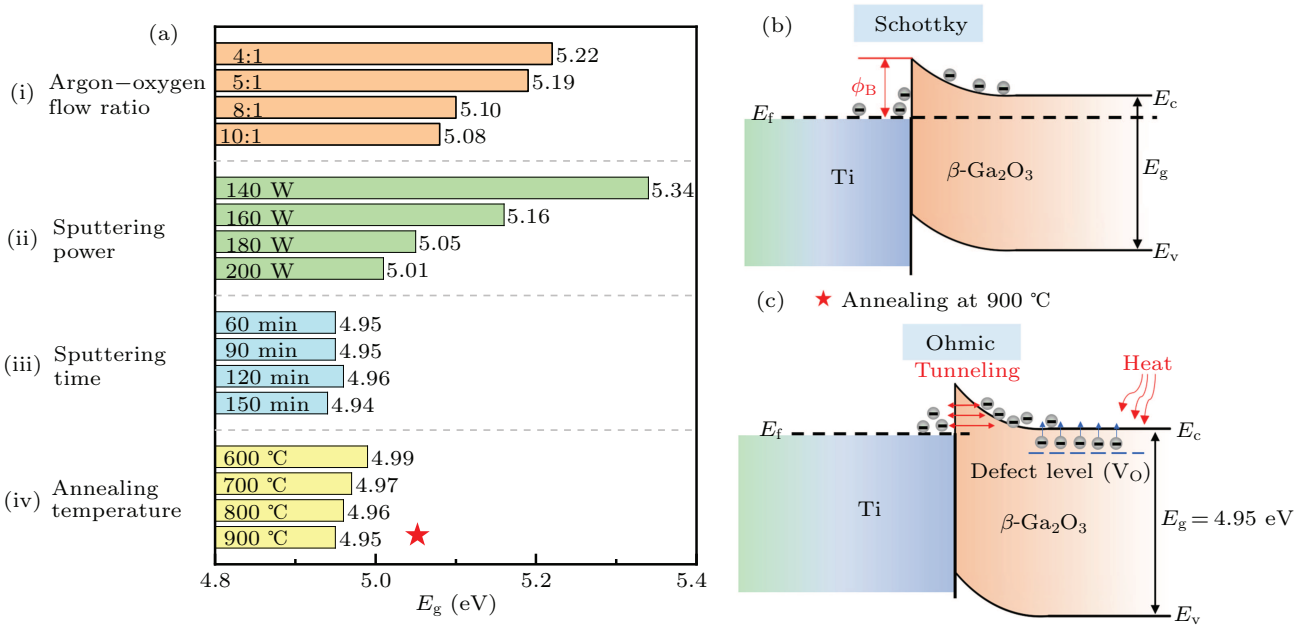


Fig. 8. (a) The E_g values of β-Ga_2O_3 thin films at different growth parameters, (b) energy band of Schottky contact between Ti and β-Ga_2O_3, and (c) mechanism for Ohmic contact formation annealed at 900 °C.

4. Conclusions

The β-Ga_2O_3 thin films are prepared on the silicon substrates by RF magnetron sputtering method. The effects of preparation parameters are studied including argon–oxygen flow ratio, sputtering power, sputtering time and annealing temperature. The annealing temperature plays a vital role in the crystallinity of the β-Ga_2O_3 film. The thickness of β-Ga_2O_3 films depend on argon–oxygen flow ratio, sputtering power and sputtering time. The surface roughness of Ga_2O_3 film increases with the augment of argon–oxygen flow ratio and sputtering time, while decreases with the sputtering power increasing. The transmission spectra of the films are tested by UV-vis, and the bandgap are calculated according to the Tauc formula. The bandgap is closely related to the quality of the film and affected by the number of oxygen vacancy defects. The Ti/Ag electrode is deposited on the surface of the films for testing the *I*–*V* curve. Ohmic contact is obtained at 900 °C, which is probably related to the transition behavior of electrons at the defect level when gain enough energy. The resistance of the film is reduced by increasing the annealing temperature because of the improved crystallinity.

Acknowledgements

Project supported by the Science and Technology Major Project of Shanxi Province, China (Grant No. 20181102013), the "1331 Project" Engineering Research Center of Shanxi Province, China (Grant No. PT201801), and the Natural Science Foundation of Shanxi Province, China (Grant No. 201801D221131).

References

[1] Tian A Q, Hu L, Zhang L Q, Liu J P and Yang H 2020 *Sci. China-Mater.* **63** 1348
[2] Chen D Z, Yuan P, Zhao S L, Liu S, Xin Q, Song X F, Yan S Q, Zhang Y C, Xi H, Zhu W D, Zhang W H, Zhang J Q, Zhou H, Zhang C F, Zhang J C and Hao Y 2022 *Sci. China-Mater.* **65** 795
[3] Huang J, Guo L W, Lu W, Zhang Y H, Shi Z, Jia Y P, Li Z L, Yang J W, Chen H X, Mei Z X and Chen X L 2016 *Chin. Phys. B* **25** 067205
[4] Higashiwaki M, Sasaki K, Kuramata A, Masui T and Yamakoshi S 2012 *Appl. Phys. Lett.* **100** 013504
[5] Higashiwaki M, Sasaki K, Murakami H, Kumagai Y, Koukitu A, Kuramata A, Masui T and Yamakoshi S 2016 *Semicond. Sci. Technol.* **31** 034001
[6] Wellenius P, Suresh A, Foreman J V, Everitt H O and Muth J F 2008 *Mater. Sci. Eng. B-Solid State Mater. Adv. Technol.* **146** 252
[7] Zhang L C, Zhao F Z, Wang F F and Li Q S 2013 *Chin. Phys. B* **22** 128502

[8] Liu Z F, Yamazaki T, Shen Y B, Kikuta T, Nakatani N and Li Y X 2008 *Sens. Actuators B-Chem.* **129** 666

[9] Jin C, Park S, Kim H and Lee C 2012 *Sens. Actuators B-Chem.* **161** 223

[10] Kim H, Jin C, An S and Lee C 2012 *Ceram. Int.* **38** 3563

[11] Yang C, Liang H W, Zhang Z Z, Xia X C, Zhang H Q, Shen R S, Luo Y M and Du G T 2019 *Chin. Phys. B* **28** 048502

[12] Arora K, Goel N, Kumar M and Kumar M 2018 *Acs Photon.* **5** 2391

[13] Wang X, Gu W F, Qiao Y F, Feng Z Y, An Y H, Zhang S H and Liu Z 2021 *Chin. Phys. B* **30** 114211

[14] Ma J, Lee O and Yoo G 2019 *IEEE J. Electron Dev. Soc.* **7** 512

[15] Ma X F, Huang Y Q, Zhi Y S, Wang X, Li P G, Wu Z P and Tang W H 2019 *Chin. Phys. B* **28** 088503

[16] Guo L L, Zhang Y M, Luan S Z, Qiao R D and Jia R X 2022 *Chin. Phys. B* **31** 017304

[17] Rao C, Fei Z Y, Chen W Q, Chen Z M, Lu X, Wang G, Wang X Z, Liang J and Pei Y L 2020 *Chin. Phys. B* **29** 097303

[18] Dong L P, Jia R X. Li C, Xin B and Zhang Y M 2017 *J. Alloys Compd.* **712** 379

[19] Sasaki K, Higashiwaki M, Kuramata A, Masui T and Yamakoshi S 2013 *IEEE Electron Device Lett.* **34** 493

[20] Shimbori A, Wong H Y and Huang A Q 2020 *Proceedings of the* 2020 32*nd International Symposium on Power Semiconductor Devices and ICs (ISPSD)*, September 13–18, 2020, Vienna Austria, p. 218

[21] Oh S, Kim C K and Kim J 2018 *Acs Photon.* **5** 1123

[22] Zhang T T, Lin J, Zhang X H, Huang Y, Xu X W, Xue Y M, Zou J and Tang C C 2013 *J. Lumines.* **140** 30

[23] Green A J, Chabak K D, Heller E R, Fitch R C, Baldini M, Fiedler A, Irmscher K, Wagner G, Galazka Z, Tetlak S E, Crespo A, Leedy K and Jessen G H 2016 *IEEE Electron Dev. Lett.* **37** 902

[24] Chen X H, Han S, Lu Y M, Cao P J, Liu W J, Zeng Y X, Jia F, Xu W Y, Liu X K and Zhu D L 2018 *J. Alloys Compd.* **747** 869

[25] Chen Y P, Liang H W, Xia X C, Shen R S, Liu Y, Luo Y M and Du G T 2015 *Appl. Surf. Sci.* **325** 258

[26] Shih H Y, Chu F C, Das A, Lee C Y, Chen M J and Lin R M 2016 *Nanoscale Res. Lett.* **11** 235

[27] Liao Y K, Jiao S J, Li S F, Wang J Z, Wang D B, Gao S Y, Yu Q J and Li H T 2018 *Crystengcomm* **20** 133

[28] Ma H L and Fan D W 2009 *Chin. Phys. Lett.* **26** 117302

[29] Dong L P, Jia R X, Xin B and Zhang Y M 2016 *J. Vac. Sci. Technol. A* **34** 060602

[30] Wang J, Ye L J, Wang X, Zhang H, Li L, Kong C Y and Li W J 2019 *J. Alloys Compd.* **803** 9

[31] Zhi Y S, Jiang W Y, Liu Z, Liu Y Y, Chu X L, Liu J H, Li S, Yan Z Y, Wang Y H, Li P G, Wu Z P and Tang W H 2021 *Chin. Phys. B* **30** 057301

[32] Holzwarth U and Gibson N 2011 *Nat. Nanotechnol.* **6** 534

[33] Liu X Z, Guo P, Sheng T, Qian L X, Zhang W L and Li Y R 2016 *Opt. Mater.* **51** 203

[34] Li S F, Jiao S J, Wang D B, Gao S Y and Wang J Z 2018 *J. Alloys Compd.* **753** 186

[35] Lu Y M, Li C, Chen X H, Han S, Cao P J, Jia F, Zeng Y X, Liu X K, Xu W Y, Liu W J and Zhu D L 2019 *Chin. Phys. B* **28** 018504

[36] Nishinaka H, Tahara D, Morimoto S and Yoshimoto M 2017 *Mater. Lett.* **205** 28

[37] Wang Y H, Li H R, Cao J, Shen J Y, Zhang Q Y, Yang Y T, Dong Z G, Zhou T H, Zhang Y, Tang W H and Wu Z P 2021 *ACS Nano* **15** 16654

[38] Mohamed M, Irmscher K, Janowitz C, Galazka Z, Manzke R and Fornari R 2012 *Appl. Phys. Lett.* **101** 132106

[39] Lee M H and Peterson R L 2021 *J. Mater. Res.* **36** 4771

[40] Lovejoy T C, Chen R Y, Zheng X, Villora E G, Shimamura K, Yoshikawa H, Yamashita H, Ueda S, Kobayashi K, Dunham S T, Ohuchi F S and Olmstead M A 2012 *Appl. Phys. Lett.* **100** 181602